Biodistribution and Radiation Dosimetry of Intraperitoneally Administered ^{124}I-Omburtamab in Patients with Desmoplastic Small Round Cell Tumors

Milan Grkovski[1], Shakeel Modak[2], Pat B. Zanzonico[1], Jorge A. Carrasquillo[3,4], Steven M. Larson[3,4], John L. Humm[1], and Neeta Pandit-Taskar[3,4]

[1]Department of Medical Physics, Memorial Sloan Kettering Cancer Center, New York, New York; [2]Department of Pediatrics, Memorial Sloan Kettering Cancer Center, New York, New York; [3]Molecular Imaging and Therapy Service, Department of Radiology, Memorial Sloan Kettering Cancer Center, New York, New York; and [4]Department of Radiology, Weill Cornell Medical College, New York, New York

The aim of this study was to assess the pharmacokinetics, biodistribution, and radiation dosimetry of ^{124}I-omburtamab administered intraperitoneally in patients with desmoplastic small round cell tumor. **Methods:** Eligible patients diagnosed with desmoplastic small round cell tumor with peritoneal involvement were enrolled in a phase I trial of intraperitoneal radioimmunotherapy with ^{131}I-omburtamab. After thyroid blockade and before radioimmunotherapy, patients received approximately 74 MBq of ^{124}I-omburtamab intraperitoneally. Five serial PET/CT scans were obtained up to 144 h after injection. Multiple blood samples were obtained up to 120 h after injection. Organ-absorbed doses were calculated with OLINDA/EXM. **Results:** Thirty-one patients were studied. Blood pharmacokinetics exhibited a biphasic pattern consisting of an initial rising phase with a median half-time (±SD) of 23 ± 15 h and a subsequent falling phase with a median half-time of 56 ± 34 h. Peritoneal distribution was heterogeneous and diffuse in most patients. Self-dose to the peritoneal cavity was 0.58 ± 0.19 mGy/MBq. Systemic distribution and activity in major organs were low. The median absorbed doses were 0.72 ± 0.23 mGy/MBq for liver, 0.48 ± 0.17 mGy/MBq for spleen, and 0.57 ± 0.12 mGy/MBq for kidneys. The mean effective dose was 0.31 ± 0.10 mSv/MBq. Whole-body and peritoneal cavity biologic half-times were 45 ± 9 and 24 ± 5 h, respectively. **Conclusion:** PET/CT imaging with intraperitoneally administered ^{124}I-omburtamab enables assessment of intraperitoneal distribution and estimation of absorbed dose to peritoneal space and normal organs before therapy.

Key Words: DSRCT; omburtamab; dosimetry; intraperitoneal; radioimmunotherapy

J Nucl Med 2022; 63:1094–1100
DOI: 10.2967/jnumed.121.262793

Desmoplastic small round cell tumor (DSRCT) is an aggressive soft-tissue sarcoma seen in adolescents and young adults (*1*). DSRCT is composed of nests of small round cells with polyphenotypic differentiation, typically a mixture of epithelial, mesenchymal, and neural features surrounded by a prominent desmoplastic stroma (*1*). This rare malignancy is associated with a t(11;22)(p13;q12) chromosomal translocation that creates the aberrant transcription factor EWS-WT1 (*2,3*). The disease primarily involves the abdomen and pelvic cavity, typically with widespread peritoneal disease. Treatment involves a multimodal approach including chemotherapy, surgery, and whole abdominopelvic radiotherapy (*4*). However, the median overall survival is low, ranging between 14 and 38 mo, with a long-term progression-free survival of < 20% (*5*), highlighting the need for novel therapeutic options to improve outcomes.

The murine monoclonal IgG1 antibody omburtamab (previously called 8H9) was developed at our institution. Omburtamab binds to the cell surface of the glycoprotein B7-H3 (CD276), which is expressed in most pediatric solid tumors, including 96% of DSRCT, whereas expression is restricted in normal tissues (*6*). Radiolabeled omburtamab using either ^{131}I or ^{124}I was developed for theranostics (*7*) and has been evaluated for the radioimmunotherapy (RIT) of leptomeningeal metastases of solid tumors including neuroblastoma by intraventricular administration (NCT00089245) (*8*) or intratumoral administration for diffuse intrinsic pontine glioma (NCT01502917) (*9*). Preclinical experiments have demonstrated that the injection of a radiolabeled agent via the intraperitoneal compartment achieved high peritoneal activities long term, high peritoneal time-integrated activity coefficients, and only limited transfer of therapeutic agents into the systemic circulation (*10*). Compartmentalized therapy with radioimmunotargeted agents facilitates delivery of higher radiation dose to the tumor target sites because of higher tumor–to–normal-tissue ratios and lower systemic activity, thereby causing lower systemic radioisotope-related toxicity (*11,12*). We have previously reported on the use of intraventricularly administered ^{124}I-omburtamab imaging for dosimetry and biodistribution assessment before therapeutic administration of ^{131}I-omburtamab (*11*).

Extending the concept of compartmental therapy with radiolabeled antibodies, we conducted a phase I study with ^{131}I-omburtamab administered intraperitoneally for therapy of patients with DSRCT and other B7-H3–expressing tumors. We demonstrated that intraperitoneal ^{131}I-omburtamab therapy is safe and can be administered in the outpatient setting. In the phase I study, treatment ^{131}I-omburtamab activities ranging from 1.11 to 3.33 GBq/m^2 were administered without significant normal-organ toxicity, and recommended phase II activity was established at 2.96 GBq/m^2 (*13*). In this report, we present in detail the biodistribution, organ uptake, and dosimetry of ^{124}I-omburtamab PET/CT imaging after intraperitoneal administration in patients with DSRCT.

Received Jun. 24, 2021; revision accepted Oct. 8, 2021.
For correspondence or reprints, contact Neeta Pandit-Taskar (pandit-n@mkscc.org).
Published online Dec. 2, 2021.

MATERIALS AND METHODS

Patients

Patients older than 1 y with a proven diagnosis of DSRCT with peritoneal involvement or other refractory or relapsed B7-H3-expressing tumors involving the peritoneum were enrolled and treated in an institutional review board–approved phase I trial (NCT01099644). All patients or their legal guardians provided written informed consent. Salient exclusion criteria were active serious infection or ≥grade 2 toxicities with the exception of myelosuppression. Patients underwent prior debulking surgery followed by insertion of an indwelling intraperitoneal catheter. Patency of the intraperitoneal catheter was maintained by twice-daily saline flushes. Intraperitoneal administration of ^{124}I-omburtamab was performed 7–14 d after catheter placement. All patients received thyroid protective medication with oral saturated solution of potassium iodide (SSKI) and liothyronine (25–75 mcg orally daily) starting 5–7 d before ^{124}I-omburtamab and continued for a total of 42 d.

^{124}I-omburtamab was radiolabeled with ^{124}I at our institutional Radiochemistry and Molecular Imaging Probes core facility and was injected within 6 h of production. After a check for good flow and patency of the intraperitoneal catheter, 74 MBq of ^{124}I-omburtamab (volume, 5.0–10.8 mL) were injected intraperitoneally over 10–15 min using a Graseby pump (Sims Graseby Ltd.) followed immediately by a 130-mL normal saline flush. This was followed 1 h later by intraperitoneal infusion of 1,200 mL/m^2 normal saline to ensure dispersion of the radioimmunoconjugate. After completion of infusion, patients were instructed to move and shift positions actively for up to 2 h to promote uniform distribution within the intraperitoneal cavity.

Pharmacokinetics and Radiation Dosimetry Assessment

Pharmacokinetic analysis for ^{124}I-omburtamab was performed using 2 modalities: blood clearance by radioassays of measured aliquots of serial blood draws and whole-body and organ activity measured by serial PET/CT scans. Blood samples for radioassay were drawn at multiple time points including 1 baseline sample before injection of the radiolabeled antibody (time 0) and at 1.1 ± 0.2 h (range, 0.9–2.0 h), 2.2 ± 0.4 h (range, 1.8–4.0 h), 4.7 ± 1.4 h (range, 2.8–8.5 h), 20.4 h, 23.9 h, and 47.8 h (range, 29.9–69.9 h) after ^{124}I-omburtamab injection. Aliquots of blood were assayed in duplicate in a scintillation well counter (LKB Wallac, Inc.) calibrated for ^{124}I and the net count rates converted to activity concentrations in percentage of the injected activity per gram. The resulting time–activity concentration data decay-corrected to the time of administration were fit to a biexponential function. The fitted biologic clearance constants were converted to effective clearance constants by incorporation of ^{124}I physical decay constant and time-integrated activity concentration calculated by analytic integration of the resulting function. The mean blood-absorbed dose was calculated by multiplying the blood time-integrated activity concentration (μCi·hr/g) by the ^{124}I energy per decay (formerly the equilibrium dose constant) for nonpenetrating radiations (Δ_{np} = 0.418 cGy·g/μCi·hr).

^{124}I-Omburtamab PET/CT Imaging. Five serial PET/CT scans were completed after the injection of ^{124}I-omburtamab up to 144 h after injection. Due to practical reasons, patients were not required to avoid voiding before first scan. All scans were obtained on a Discovery STE or 710 PET/CT scanner (GE Healthcare) using the ^{124}I decay parameters (positron yield, 0.23; half-life, 4.18 d).

The field of imaging included vertex to the mid-thigh. The acquisition time was 5 min per field of view. PET emission data were corrected for attenuation, scatter, and random events using the vendor-supplied corrections. The CT scan of the PET/CT was mainly for attenuation correction and was obtained using a combination of ultralow (10 mA) and low mA (40–80 mA based on body weight) with 140 keV for the multiple scanning times. The CT dose ranged from 9.2 to 18.4 mSv in patients. Images were reconstructed using standard clinical reconstruction parameters: ordered-subset expectation maximization using 2 iterations with 16 subsets and a gaussian postprocessing filter with a full width half maximum of 6.0 mm.

Organ Dosimetry Calculation

Absorbed doses to total body and individual organs were calculated on the basis of the time–activity data derived from each patient's set of PET/CT images. Volumes of interest were drawn manually over normal organs (heart, liver, spleen, kidneys, stomach contents, thyroid, gastrointestinal tract, and peritoneal cavity) and whole body in Hybrid Viewer (HERMES Medical Solution, Inc.). Volumes of interest were placed on PET images using corresponding CT and fused PET/CT image guidance. The decay-corrected mean activity concentrations [A(t)] (in kBq/cc) in all investigated organs were each fit to a mathematic function of the following form:

$$[A(t)] = [A_{plateau}]\left(1 - \exp\left(-\left(0.693/T_{uptake}\right)\times t\right)\right)\exp\left(\left(-0.693/T_{clearance1}\right)\times t\right).$$

The decay-corrected total-body activity concentrations were each fit to a mathematic function of the following form:

$$[A(t)] = [Ao]\exp\left(\left(-0.693/T_{clearance2}\right)\times t\right),$$

where t is the time after administration; $[A_{plateau}]$ is the plateau activity concentration in the investigated organs; T_{uptake} and $T_{clearance1}$ are the uptake and clearance half-times, respectively, in the investigated organs; [Ao] is the zero-time–activity concentration in total-body; and $T_{clearance2}$ is the clearance half-time in the total body. The foregoing fitted time–activity functions were integrated analytically from t = 0 (i.e., the time of injection) to time t = ∞ (i.e., the time of complete radioactive decay), incorporating the physical half-life of ^{124}I (4.18 d = 100.3 h) into the respective decay-corrected uptake T_{uptake} and clearance half-times, $T_{clearance1}$ and $T_{clearance2}$. The resulting time-integrated activity concentrations were converted to total-organ time-integrated activities by multiplying by the corresponding organ masses in the Reference Man anatomic model (*14*) closest in total-body mass to that of the patient and then to time-integrated activity coefficients by dividing by the administered activity. These time-integrated activity coefficients were entered into the OLINDA/EXM 1.1 radiation dosimetry program (*14*), with ^{124}I as the radionuclide and the Reference Man anatomic model closest in age to that of the patient selected. For adult patients, both female and male models were used. A peritoneal cavity model (*15,16*) as implemented in OLINDA/EXM was applied.

RESULTS

Patients

Thirty-one patients (26 men and 5 women; age, 21 ± 8 y; age range, 8–38 y) received ^{124}I-omburtamab and underwent 4 (all patients) or 5 (20 patients) PET/CT scans. The mean injected activity was 73 ± 3 MBq (range, 65–77 MBq). The mean times for PET/CT scan acquisitions were 3.6 ± 0.8 (range, 2.4–5.4), 22.3 ± 2.5 (range, 17.6–27.0), 46.4 ± 2.6 (range, 42.5–52.3), 69.0 ± 1.4 (range, 66.1–71.7), and 125.1 ± 14.9 (range, 114.1–171.2) h after injection of ^{124}I-omburtamab.

Biodistribution

Imaging showed localization of tracer in the peritoneal cavity dispersed within 4 quadrants of the abdomen and pelvis and cleared over time as noted on serial imaging (Fig. 1). The distribution was heterogeneous, with prominent activity noted in most patients in the bilateral paracolic gutters, lower abdomen, and pelvis.

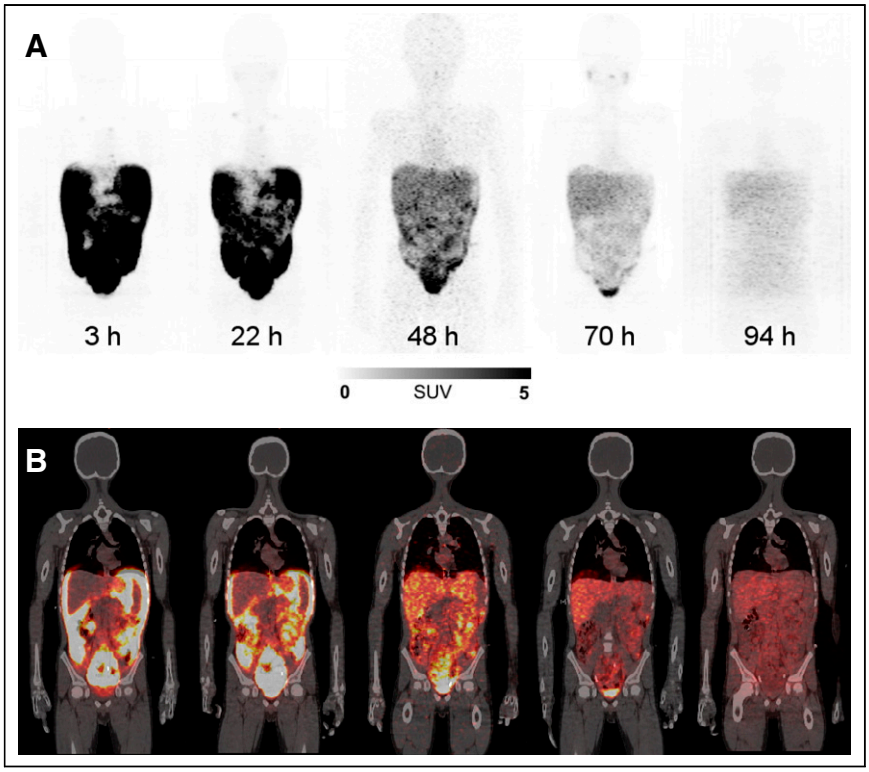

FIGURE 1. ^{124}I-omburtamab imaging. Maximum-intensity-projection (A) and coronal (B) images after ^{124}I-omburtamab injection. Cardiac blood-pool activity is low at all time points. Peritoneal distribution is most intense initially and decreasing with time. Mild activity in salivary glands is noted in later images.

In 4 patients, the distribution was noted in all quadrants but with asymmetric increased activity in either the right or the left abdomen. In 3 patients, the activity showed a more localized pattern in the lower abdomen and pelvis, although distribution was noted in all quadrants. Overall, radiotracer activity in the peritoneum decreased with time, with an average biologic half-time of 24 ± 5 (range, 18–45) h. Perihepatic uptake in the peritoneum was variable, with moderate to intense uptake seen in 10 patients whereas others showed mild or minimal activity (Fig. 2). Moderate to prominent uptake was noted in the peritoneum superiorly around the spleen in all patients (Fig. 2). Minimal (barely discernible) to mild uptake was observed in the cardiac blood pool that initially increased within 24–72 h and later decreased as noted in delayed imaging (Figs. 1 and 2). Minimal activity was noted within the liver or spleen parenchyma in the initial 48 h. Mild activity was noted in the salivary glands for all patients. Thyroid activity was minimal to mild in all patients (Fig. 1), except in 2 patients. These 2 patients had prominent activity in the thyroid and known prior hypothyroidism; in 1 patient, this was related to underlying chronic thyroiditis (Fig. 2). The uptake in the thyroid generally increased with time up to 72 h, after which the activity decreased. Bladder contents activity was noted as early as the first PET/CT scan in many patients.

^{124}I-omburtamab activity in the lymph nodes was observed in 24 patients in early imaging at 22 h after injection and in 17 patients at 125 h after injection. The nodal visualization included internal mammary (76% of cases), supraclavicular (57% of cases), and mediastinal nodes (52% of cases). Also observed were paratracheal, subcarinal, preaortic, cervical, subaortic, pretracheal, substernal, intrathoracic, paraesophageal, periportal, and retroclavicular lymph nodes. An example patient with nodal uptake is shown in Figure 2. Activity in the lung in the pleural–diaphragmatic region and posteriorly in the lung periphery and pleural region was noted in some patients, primarily in those who showed ipsilateral nodal activity.

Time–activity curves for normal organs revealed a gradual increase in radioactivity (quantified as ^{124}I-omburtamab SUV_{mean} normalized by body weight) in heart blood pool, liver, and kidneys, reaching a plateau between 24 and 48 h after injection and subsequently decreasing (Fig. 3; detailed information is provided in Supplemental Table 1 [supplemental materials are available at http://jnm.snmjournals.org]). Although splenic parenchyma activity was generally very low, uptake was highest in the first PET/CT scan and decreased thereafter. The uptake in stomach contents increased initially, being most prominent at 24 h, and decreased thereafter. Bladder contents activity was noted as early as the first scan and was variably seen in subsequent scans in all patients, suggesting renal excretion. ^{124}I-omburtamab cleared from intraperitoneal space exponentially, with an SUV_{mean} of 10 ± 1 at 4 h after injection (range, 7–19) and falling to 0.5 ± 0.1 at 125 h after injection (range, 0.2–0.9). The SUV_{max} in the peritoneal space also exhibited a similar pattern, decreasing from 53 ± 14 (range, 14–114) at 4 h after injection to 2.2 ± 0.5 (range, 0.2–4.6) at 125 h after injection.

Kinetic Analysis

Blood pharmacokinetics in 28 patients showed a biphasic pattern consisting of an initial rising phase with a median half-time of 23 ± 15 h and a subsequent falling phase with a median half-time of 56 ± 34 h. Blood activity reached a plateau after 24 h, approaching a maximum of 1.8 percentage of injected activity per liter (Fig. 4B).

The whole-body clearance conformed to a monoexponential function (Fig. 4A). Mean whole-body biologic half-time was 45 ± 9 h, and time-integrated activity coefficients for whole body and peritoneal cavity were 44 ± 6 and 20 ± 7 h, respectively (Table 1). ^{124}I-omburtamab organ dosimetry is summarized in Table 2. Median absorbed dose to the peritoneum was 0.58 mGy/MBq. The mean absorbed doses were 0.72 ± 0.23 mGy/MBq for liver, 0.48 ± 0.17 mGy/MBq for spleen, 0.57 ± 0.12 mGy/MBq for kidneys, 0.84 ± 0.29 mGy/MBq for urinary bladder wall, and 0.19 ± 0.05 mGy/MBq for lungs. The radiation dose to the thyroid was 0.25 ± 0.19 mGy/MBq (mean ± SD) for all patients except the 2 with prior hypothyroidism whose thyroid-stimulating hormone could not be suppressed. Time-integrated activity coefficients and normal-organ dosimetry for 3 subgroups based on patient age are summarized in Supplemental Tables 2 and 3.

The estimated mean effective dose was 0.31 ± 0.10 mSv/MBq. The total dose to blood from the 73 MBq of ^{124}I-omburtamab

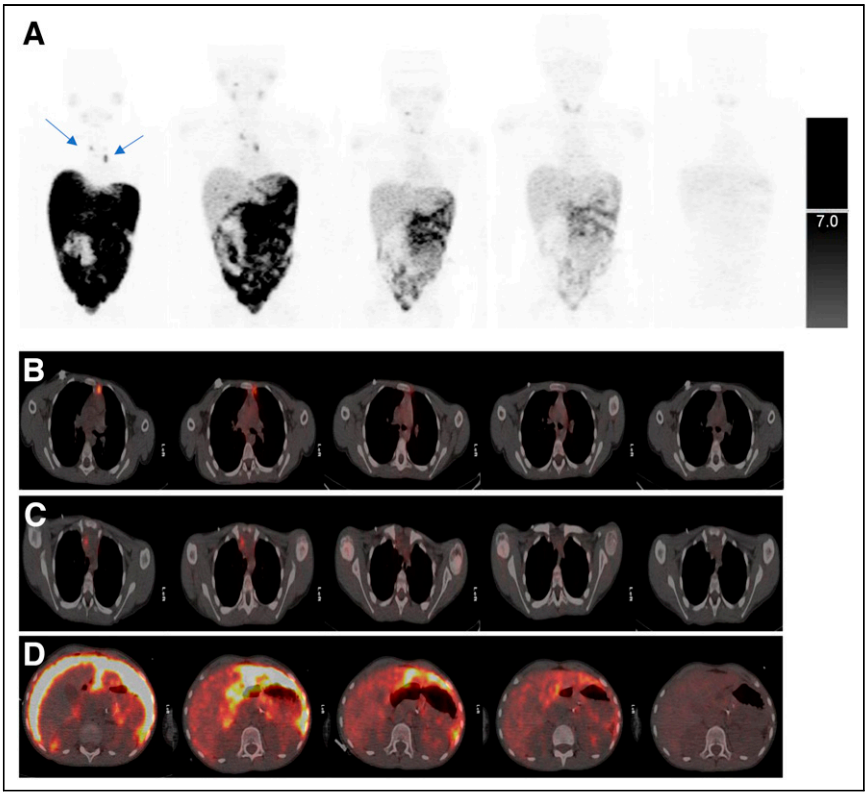

FIGURE 2. Serial images after ^{124}I-omburtamab injection. Maximum-intensity-projection (A) and fused transaxial images PET/CT images (B–D). Peritoneal activity is intense (A and D). Distribution is noted along all quadrants with slightly more in bilateral paracolic gutters. Peritoneal distribution decreases with time along with increasing blood-pool activity and thyroid uptake in later images that decreases in last image. Right supraclavicular and mediastinal lymph nodes are visualized in early images (arrows), demonstrating decreased visualization with time.

injection, as calculated from blood sample data, was 1.1 ± 0.6 cGy (range, 0.2–3.1) or 0.15 ± 0.08 mGy/MBq (range, 0.02–0.42).

DISCUSSION

We have used ^{131}I- or ^{124}I-labeled 8H9/omburtamab antibody theranostically for localized compartmental therapies with intraventricular/intrathecal administration for metastatic leptomeningeal disease in neuroblastoma or other B7-H3–expressing tumors (*8,12*). Both ^{131}I-omburtamab and ^{124}I-omburtamab have an advantage as theranostic agents, as imaging allows for assessment of individual patient activity distribution and dosimetric estimation for radiation absorbed doses for both normal tissues and tumors before therapy (*11*). An additional advantage of ^{124}I-omburtamab is imaging with PET/CT scanners that have higher resolution allows for quantitation that is easier and more accurate than γ-camera imaging. Omburtamab is a highly specific antibody that targets B7-H3, an antigen expressed in several tumors including most DSRCTs, making it an attractive target for radioimmunotherapy (*6*), as noted in early preclinical studies (*7,10*). We have developed radiolabeled omburtamab and treated patients with ^{124}/^{131}I-omburtamab in 3 phase I/II trials using compartmental delivery systems, namely, peritoneal cavity (intraperitoneal infusions), cerebrospinal fluid space (intraventricular/intrathecal injections), or localized intratumoral delivery using a convection-enhanced delivery method in patients with diffuse intrinsic pontine glioma (*7–9*). We have shown the feasibility and use of ^{124}I-omburtamab imaging for biodistribution and dosimetry assessment and as a theranostic (*9*). Intraperitoneal RIT has the potential to deliver higher radiation doses to the tumor while limiting systemic organ and blood doses to low radiation doses (*16*).

For DSRCT, which primarily involves the peritoneum, we used intraperitoneal administration of RIT and showed the safety of intraperitoneal ^{131}I-omburtamab RIT (*13*). Patients receiving doses of ^{131}I-omburtamab up to 3.33 GBq/m^2 (90 mCi/m^2) did not exhibit major toxicities, and all toxicities were reversible without intervention. Intraperitoneal RIT appeared to be associated with a decreased risk of abdominopelvic DSRCT relapse compared with historical data, with 9 of 23 patients receiving the recommended phase II activity dose of 2.96 GBq/m^2 being alive disease-free at a median follow up of 42 mo after RIT. Here we present details of the ^{124}I-omburtamab PET/CT imaging used for assessment of biodistribution and radiation dosimetry of normal organs and examine its potential for treatment planning.

In this phase I study, ^{124}I-omburtamab imaging before ^{131}I-omburtamab intraperitoneal radioimmunotherapy showed favorable biodistribution with dispersion within all quadrants of the peritoneal cavity and low systemic activity in other organs. The peritoneal distribution was heterogeneous but localized in all 4 quadrants of the abdomen in all patients. There was no clear pattern of variation of distribution noted in patients. The overall retention time in the peritoneum was long (mean biologic half-time of 24.5 ± 5.2 h). The dosimetry estimates showed low normal-organ doses. The assessment of organ uptake enabled assessment of projected dosimetry with ^{131}I-omburtamab (*13*). Because most patients had surgical debulking and were required to have no measurable disease, any specific tumor dosimetry estimation could not be performed.

Uptake of ^{124}I-omburtamab in major organs such as the liver and spleen was low (maximum uptake of ~0.003 percentage of the injected activity per gram for both), reflecting slow systemic distribution of the tracer, as also noted by low cardiac blood-pool activity over all imaging time points and low cross-reactivity with normal tissues. The uptake pattern of the organs showed an initial increase, suggesting slow systemic absorption from intraperitoneal activity, followed by clearance that paralleled the blood activity, which also showed an initial increase before clearance. The low systemic absorption resulted in low blood and bone marrow exposures. The elimination pathway appears to be primarily renal, as suggested by urine activity within the bladder, low liver activity, and lack of gallbladder or gastrointestinal tract activity, suggesting that hepatobiliary clearance was not prominent. Thyroid doses were overall low. Two patients with underlying hypothyroidism had higher doses likely

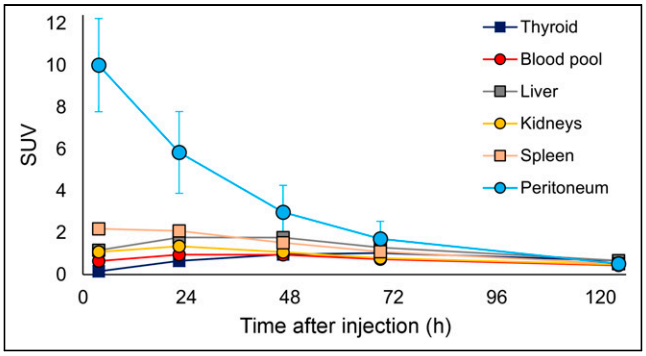

FIGURE 3. Mean SUV_{bw} for normal organs and peritoneum (n = 31 patients).

due to inherent high thyroid-stimulating hormone stimulation. Clinical follow-up with measured thyroid-stimulating hormone did not reveal hypothyroidism resulting from ^{131}I-omburtamab therapy in any patients (*13*).

Lymph node uptake was variable; the nodes visualized were not metastatic as assessed by concurrent or follow-up diagnostic CT scans. The significance of the nodal uptake is unclear, however. In many patients who showed nodal uptake, activity was noted along the pleuroperitoneal surface, as was diffuse uptake along inferior posterior aspects of the pleura on the ipsilateral side of the nodal uptake, suggesting a likely mechanism related to transit of ^{124}I-omburtamab along the lymphatics and thoracic duct to mediastinal nodes (*17*). Overall, the normal-organ and whole-body radiation dosimetry profile of imaging with ^{124}I-omburtamab patients was favorable, with low uptake and radiation absorbed doses noted. The total body effective dose was 0.3 mSv/MBq for intraperitoneal administration, which is similar or slightly lower than the approximately 0.5 mSv/MBq noted after intraventricular administration of ^{124}I-omburtamab in 42 patients with metastatic leptomeningeal tumors (*11*) and with convection-enhanced intratumoral delivery in patients with diffuse intrinsic pontine glioma (NCT01502917). Peritoneal-to-liver and peritoneal–to–blood-pool SUV ratios were very high (12 ± 9 and 21 ± 10, respectively, on the first PET/CT).

TABLE 1
Time-Integrated Activity Coefficients (h) for Selected Organs for Intraperitoneal Administration of ^{124}I-Omburtamab

Organ	Mean	SD	Median	Minimum	Maximum
Liver	3.5	1.6	3.1	1.5	7.3
Kidneys	0.4	0.1	0.4	0.3	0.7
Spleen	0.3	0.2	0.3	0.1	0.7
Stomach*	0.9	0.5	0.7	0.3	2.1
Urinary bladder*	1.1	0.5	1.0	0.3	2.9
Thyroid	0.07	0.21	0.01	0.00	1.22
Peritoneal cavity†	20.4	6.9	19.2	9.0	32.6
Rest of body	17.3	7.7	17.8	3.8	34.6
Whole-body	44.3	6.0	44.1	34.2	57.4

*Dose for cavity/content.
†Dose to peritoneal cavity wall per disintegration in peritoneal cavity.

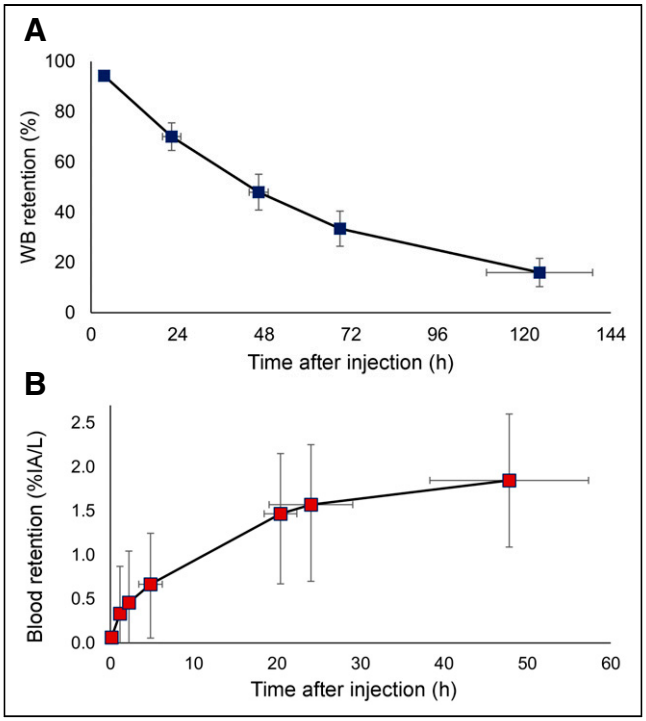

FIGURE 4. Whole-body (WB) (A) and blood (B) clearance of ^{124}I-omburtamab displayed in aggregate decay-corrected mean values. %IA = percentage injected activity. Mean ± SD.

^{124}I-omburtamab imaging allows assessment of biodistribution and dosimetry before intraperitoneal delivery of ^{131}I-omburtamab antibody for therapy. In this phase I study, ^{124}I-omburtamab imaging was used to predict organ and peritoneal doses from therapeutic administration of ^{131}I-omburtamab (*13*). Our study used PET/CT imaging to derive dose estimates for intraperitoneal RIT, unlike prior studies that used radioimmunoconjugates targeting surface antigens and assessed biodistribution and dosimetry either by γ-camera imaging or external radiation probes as applied, for example, to single-photon emitters such as β-emitting ^{90}Y or α-emitting ^{211}At and ^{212}Pb for therapy (*18–21*). In our study, pediatric and adolescent patients with DSRCT scheduled to undergo treatment with ^{131}I-omburtamab were imaged with companion theranostic positron-emitting radioimmunoconjugate ^{124}I-omburtamab. This allowed for more comprehensive quantitative imaging at multiple time points with higher spatial resolution than γ-camera imaging performed in other studies of intraperitoneal RIT. The predicted doses of ^{131}I-omburtamab for intraperitoneal radioimmunotherapy were within acceptable normal-organ limits, and therapy was well tolerated by all DSRCT patients with no dose-limiting toxicities noted (*13*). The systemic activity and blood and organ radiation doses were low from both ^{124}I-omburtamab and ^{131}I-omburtamab, favoring use of this theranostic pair for compartmental intraperitoneal radioimmunotherapy. On the basis of these encouraging data, we have initiated a phase II study of ^{131}I-omburtamab–based intraperitoneal RIT in

TABLE 2
Normal-Organ Absorbed Dose and Effective Dose Estimates for Intraperitoneal Administration of ^{124}I-Omburtamab

Mean absorbed doses (mGy/MBq)	Mean	SD	Median	Minimum	Maximum
Adrenals	0.45	0.07	0.44	0.27	0.59
Brain	0.09	0.06	0.08	0.02	0.21
Breasts	0.12	0.04	0.11	0.07	0.21
Gallbladder wall	0.21	0.07	0.20	0.10	0.36
Lower large intestine wall	0.23	0.06	0.21	0.15	0.35
Small intestine	0.50	0.09	0.48	0.30	0.68
Stomach wall	0.66	0.16	0.65	0.44	1.10
Upper large intestine wall	0.46	0.08	0.46	0.28	0.62
Heart wall	0.39	0.07	0.38	0.26	0.53
Kidneys	0.57	0.12	0.55	0.38	0.80
Liver	0.73	0.22	0.68	0.41	1.26
Lungs	0.19	0.05	0.17	0.13	0.30
Muscle	0.20	0.05	0.18	0.14	0.30
Ovaries	0.40	0.02	0.40	0.36	0.41
Pancreas	1.07	0.26	1.03	0.59	1.54
Red marrow	0.22	0.04	0.21	0.15	0.30
Osteogenic cells	0.25	0.07	0.23	0.16	0.38
Skin	0.11	0.04	0.10	0.06	0.19
Spleen	0.48	0.17	0.50	0.22	1.00
Testes	0.13	0.06	0.11	0.06	0.25
Thymus	0.15	0.05	0.13	0.08	0.25
Thyroid	0.27	0.24	0.19	0.07	1.03
Urinary bladder wall	0.85	0.29	0.78	0.36	1.52
Uterus	1.21	0.21	1.14	1.00	1.50
Total body	0.22	0.05	0.21	0.15	0.32
Peritoneum self-dose	0.57	0.19	0.57	0.22	1.07
Effective dose (mSv/MBq)	0.31	0.10	0.30	0.20	0.71

Units are mGy/MBq unless otherwise noted.

combination with external-beam radiotherapy for DSRCT and other B7-H3–expressing tumors involving the peritoneum (NCT04022213).

CONCLUSION

PET/CT imaging with intraperitoneally administered ^{124}I-omburtamab enables the assessment of both intraperitoneal and systemic distribution, allowing for estimation of absorbed dose to the peritoneum and normal organs before therapy.

DISCLOSURE

This work was supported by funding from Taybandz, Steven Vanover Foundation, Sarcoma SPORE, and the NIH/NCI Cancer Center Support Grant P30 CA008748. Milan Grkovski reports personal fees from Y-mAbs Therapeutics, Inc. unrelated to the submitted work. Neeta Pandit-Taskar is or has served as a consultant and advisory board member and has received honoraria from Actinium Pharma, Progenics, Medimmune/AstraZeneca, Illumina, Imaginab, and Y-mAbs and conducts research institutionally supported by Y-mAbs, Imaginab, Bristol Myers Squibb, Bayer, Clarity Pharma, Janssen, and Regeneron. Shakeel Modak has a consulting or advisory role for Y-mAbs Therapeutics and Illumina RP and has 2 patents pending with no financial benefit. Pat B. Zanzonico, Jorge A. Carrasquillo, Steven M. Larson, and John L. Humm have a consulting or advisory role with Y-mAbs Therapeutics. No other potential conflict of interest relevant to this article was reported.

ACKNOWLEDGMENTS

We thank our institutional nuclear medicine research nurses, radiopharmacy, technologists, radiation safety, surgical team, and inpatient nurse practitioners for their work in patient care.

KEY POINTS

QUESTION: What is the feasibility, safety, and clinical utility of ^{124}I-omburtamab PET/CT imaging for patients with DSRCT?

PERTINENT FINDINGS: In this phase I study, 31 patients were imaged with ^{124}I-omburtamab administered intraperitoneally before treatment with ^{131}I-omburtamab. Dosimetry and biodistribution were favorable, with minimal uptake in organs and long retention in the peritoneal cavity.

IMPLICATIONS FOR PATIENT CARE: ^{124}I-omburtamab PET/CT enables theranostic imaging assessment in patients and has a potential role in planning therapy. A phase II study is under way.

REFERENCES

1. Mora J, Modak S, Cheung NK, et al. Desmoplastic small round cell tumor 20 years after its discovery. *Future Oncol.* 2015;11:1071–1081.
2. Sawyer JR, Tryka AF, Lewis JM. A novel reciprocal chromosome translocation t(11;22)(p13;q12) in an intraabdominal desmoplastic small round-cell tumor. *Am J Surg Pathol.* 1992;16:411–416.
3. Ladanyi M, Gerald W. Fusion of the EWS and WT1 genes in the desmoplastic small round cell tumor. *Cancer Res.* 1994;54:2837–2840.
4. Quaglia MP, Brennan MF. The clinical approach to desmoplastic small round cell tumor. *Surg Oncol.* 2000;9:77–81.
5. Lal DR, Su WT, Wolden SL, Loh KC, Modak S, La Quaglia MP. Results of multimodal treatment for desmoplastic small round cell tumors. *J Pediatr Surg.* 2005; 40:251–255.
6. Modak S, Kramer K, Gultekin SH, Guo HF, Cheung NK. Monoclonal antibody 8H9 targets a novel cell surface antigen expressed by a wide spectrum of human solid tumors. *Cancer Res.* 2001;61:4048–4054.
7. Modak S, Guo HF, Humm JL, Smith-Jones PM, Larson SM, Cheung NK. Radioimmunotargeting of human rhabdomyosarcoma using monoclonal antibody 8H9. *Cancer Biother Radiopharm.* 2005;20:534–546.
8. Kramer K, Kushner BH, Modak S, et al. Compartmental intrathecal radioimmunotherapy: results for treatment for metastatic CNS neuroblastoma. *J Neurooncol.* 2010;97:409–418.
9. Souweidane MM, Kramer K, Pandit-Taskar N, et al. Convection-enhanced delivery for diffuse intrinsic pontine glioma: a single-centre, dose-escalation, phase 1 trial. *Lancet Oncol.* 2018;19:1040–1050.
10. Modak S, Gerald W, Cheung NK. Disialoganglioside GD2 and a novel tumor antigen: potential targets for immunotherapy of desmoplastic small round cell tumor. *Med Pediatr Oncol.* 2002;39:547–551.
11. Pandit-Taskar N, Zanzonico PB, Kramer K, et al. Biodistribution and dosimetry of intraventricularly administered ^{124}I-omburtamab in patients with metastatic leptomeningeal tumors. *J Nucl Med.* 2019;60:1794–1801.
12. Kramer K, Pandit-Taskar N, Zanzonico P, et al. Low incidence of radionecrosis in children treated with conventional radiation therapy and intrathecal radioimmunotherapy. *J Neurooncol.* 2015;123:245–249.
13. Modak S, Zanzonico P, Grkovski M, et al. B7H3-directed intraperitoneal radioimmunotherapy with radioiodinated omburtamab for desmoplastic small round cell tumor and other peritoneal tumors: results of a phase I study. *J Clin Oncol.* 2020: JCO.20.01974.
14. Stabin MG, Sparks RB, Crowe E. OLINDA/EXM: the second-generation personal computer software for internal dose assessment in nuclear medicine. *J Nucl Med.* 2005;46:1023–1027.
15. Watson EE, Stabin MG, Davis JL, Eckerman KF. A model of the peritoneal cavity for use in internal dosimetry. *J Nucl Med.* 1989;30:2002–2011.
16. Larson SM, Carrasquillo JA, Colcher DC, et al. Estimates of radiation absorbed dose for intraperitoneally administered iodine-131 radiolabeled B72.3 monoclonal antibody in patients with peritoneal carcinomatoses. *J Nucl Med.* 1991;32: 1661–1667.
17. Parungo CP, Soybel DI, Colson YL, et al. Lymphatic drainage of the peritoneal space: a pattern dependent on bowel lymphatics. *Ann Surg Oncol.* 2007;14:286–298.
18. Alvarez RD, Huh WK, Khazaeli MB, et al. A phase I study of combined modality ^{90}Yttrium-CC49 intraperitoneal radioimmunotherapy for ovarian cancer. *Clin Cancer Res.* 2002;8:2806–2811.
19. Oei AL, Verheijen RH, Seiden MV, et al. Decreased intraperitoneal disease recurrence in epithelial ovarian cancer patients receiving intraperitoneal consolidation treatment with yttrium-90-labeled murine HMFG1 without improvement in overall survival. *Int J Cancer.* 2007;120:2710–2714.
20. Cederkrantz E, Andersson H, Bernhardt P, et al. Absorbed doses and risk estimates of ^{211}At-MX35 F(ab')2 in intraperitoneal therapy of ovarian cancer patients. *Int J Radiat Oncol Biol Phys.* 2015;93:569–576.
21. Hallqvist A, Bergmark K, Bäck T, et al. Intraperitoneal α-emitting radioimmunotherapy with ^{211}At in relapsed ovarian cancer: long-term follow-up with individual absorbed dose estimations. *J Nucl Med.* 2019;60:1073–1079.